NANOSYSTEMS:
PHYSICS, CHEMISTRY, MATHEMATICS

Chupakhina T.I., et al. *Nanosystems: Phys. Chem. Math.*, 2024, **15** (4), 540–547.
http://nanojournal.ifmo.ru
DOI 10.17586/2220-8054-2024-15-4-540-547

Original article

Study of photocatalytic activity in two light ranges of $Sr_2Mn_{0.4}Ti_{0.6}O_4$ oxide with the K_2NiF_4-type structure

Tatyana I. Chupakhina[1,a], Olga I. Gyrdasova[1,b], Anastasya M. Uporova[1], Larisa Y. Buldakova[1], Mikhail Y. Yanchenko[1], Dzhavid V. Mamedov[2], Yulia A. Deeva[1], Inna V. Baklanova[1]

[1]Institute of Solid State Chemistry UB RAS, Ekaterinburg, Russia

[2]Zavoisky Physical-Technical Institute, FRC Kazan Scientific Center of RAS, Kazan, Russia

[a]chupakhina@yandex.ru, [b]gyrdasova@ihim.uran.ru

Corresponding author: Tatyana I. Chupakhina, chupakhina@yandex.ru

PACS 82.65.+r

ABSTRACT The photocatalytic properties of single-phase sample $Sr_2Mn_{0.4}Ti_{0.6}O_4$ is studied as a representative of a series of $Sr_2Mn_xTi_{1-x}O_4$ solid solutions ($x = 0.05, 0.15, 0.25, 0.4$) obtained by the SHS. The sample annealed at 1200 °C is characterized by a uniform distribution of Sr, Ti and Mn in the oxidation degree (4+) inside the aggregates, the average size of which does not exceed 1 μm. According to UV-Vis-NIR spectroscopy data, a narrowing of the band gap of Sr_2TiO_4 from 3.16 to 1.8 eV is observed when it is doped with 40 mol% of manganese. This is due to the high photoactivity of $Sr_2Mn_{0.4}Ti_{0.6}O_4$ in the HQ oxidation reaction in UV and blue light.

KEYWORDS nanostructured strontium titanate, Raddlesden–Popper structures, oxidative photocatalysis

ACKNOWLEDGEMENTS The work was supported by RCF, project No. 24-23-20123. The UV-Vis-NIR spectrum was recorded on equipment of the Center for Joint Use "Spectroscopy and Analysis of Organic Compounds" at the Postovsky Institute of Organic Synthesis, UB RAS.

FOR CITATION Chupakhina T.I., Gyrdasova O.I., Uporova A.M., Buldakova L.Y., Yanchenko M.Y., Mamedov D.V., Deeva Y.A., Baklanova I.V. Study of photocatalytic activity in two light ranges of $Sr_2Mn_{0.4}Ti_{0.6}O_4$ oxide with the K_2NiF_4-type structure. *Nanosystems: Phys. Chem. Math.*, 2024, **15** (4), 540–547.

1. Introduction

The complex oxide Sr_2TiO_4 with layered Raddlesden–Popper structure ($A_{n+1}B_nO_{3n+1}$, $n = 1$, structural type K_2NiF_4) have high dielectric constant and low dielectric loss angle tangent. Strontium titanates are wide-gap semiconductors which are used in various fields of electronic engineering: electro-optical devices, multilayer capacitors and thermistors [1]. Sr_2TiO_4-based compounds find practical application in photosystems [2, 3] as photocatalysts in the process of H_2 evolution from H_2O [4] or oxidation of toxic organic compounds to carbon dioxide and water [5]. Phenol derivatives are life-threatening pollutants of water resources. Titanium dioxide as a photocatalyst in the form of anatase/rutile structural mixture is traditionally used to decompose benzene-containing pollutants [6] and 1.4-dihydroxybenzene (hydroquinone) (60 %) n-benzoquinone and catechol are the main intermediates during phenol photooxidation by TiO_2 catalyst [7]. The hydroquinone oxidation reaction may be considered as a model process for photooxidation reaction of phenolic compounds. The main problem of using TiO_2 in photostimulated processes for removal of toxic contaminants is its limited spectral range of operation (UV region).

Structural analogs of TiO_2 in the anatase phase are strontium titanates. The band gaps of Sr_2TiO_4 and TiO_2 are comparable ($\sim$ 3.3 eV) [8]. Therefore, compounds based on Sr_2TiO_4 can become an alternative to the known catalysts (Degussa). At the same time, crystalline Sr_2TiO_4, like TiO_2, shows photoactivity only under irradiating by light with wavelength $\lambda_{\max} = 253$ nm (UV range) [8].

There is extensive information on methods of surface activation of perovskite-like oxides with description of various synthesis technologies, creation of composite structures, and design of heterostructures [9–14]. The main way to expand the spectral working range of strontium titanates is doping with d-metals in position B, as well as increasing the working surface area [9–13]. It is known that doping with transition elements like Mn, leads to enhanced light absorption ability of strontium titanates due to the effective reduction of the band gap. Thus, doping of perovskite-like structure strontium titanate with 1 and 3 at.% Mn increases its photocatalytic activity in the decomposition of methylene blue, and the oxide with lower Mn content is more effective as a catalyst [13]. In contrast, [14] found that in $SrTi_{1-x}Mn_xO_3$ ($x = 0.05$ – 0.2), the sample with $x = 0.15$ was found to be a more efficient catalyst for the decomposition of methylene blue.

There is no information on the application of manganese-containing layered perovskites based on Sr_2TiO_4 in photocatalysis. There are also no studies in the field of using doped strontium titanates with the structure of the first and second homologues of the Radlesden–Popper series as photocatalysts for the decomposition of phenolic compounds.

Thus, the goal was to synthesize $Sr_2Ti_{1-x}Mn_xO_4$ ($0.05 \leq x \leq 0.4$) solid solutions and investigate their activity in the photooxidation of 1.4-dihydroxybenzene (hydroquinone).

By changing the doping of Sr_2TiO_4 and the conditions of its production, it is possible to extend its photosensitivity to the visible range of spectrum.

Practically significant properties of such materials (specific surface area, degree of defectivity, porosity, size, morphology and internal architecture of aggregates) are set by synthesis. The authors propose a comprehensive solution to these problems by precursor synthesis method The technology of salt composites pyrolysis was used for preparation of complex oxides with various composition (method of self-propagating high-temperature synthesis, SHS) [15, 16].

In this work, complex oxide $Sr_2Mn_{0.4}Ti_{0.6}O_4$ with K_2NiF_4-type structure was generated by SHS method. Its catalytic properties were studied in the photooxidation reaction with 1.4-dihydroxybenzene (hydroquinone, HQ) when the sample was exposed to radiation with wavelengths of $\lambda_{\max} = 253$ nm (UV range) and $\lambda_{\max} = 440 - 460$ nm (visible blue).

2. Experimental

Reagents used are as follows: strontium nitrate $Sr(NO_3)_2$ (high purity), titanium tetraisopropoxide $Ti(i\text{-}OC(CH_3)_2)_4$ ($\rho = 0.963$ g/cm^3) and manganese (II) nitrate $Mn(NO_3)_2 \cdot 4H_2O$ (high purity). C_2H_5OH 96 % and HNO_3 (high purity) were used as solvents. As an organic reducing agent for the initiation of the fuel process in a mixture of nitrates, $(NH_4)_2C_6H_6O_7$ (high purity) was used. $Sr_2Mn_{0.4}Ti_{0.6}O_4$ was prepared by SHS method according to the procedure described in [16]. The final single-phase oxide $Sr_2Mn_xTi_{1-x}O_4$ was obtained by annealing the SHS product at a temperature of 1200 °C during 8 h.

X-ray powder diffraction (XRD-7000 diffractometer, Shimadzu, Japan) using CuKα radiation in the 2θ range 5 to 80° with a step of 0.03° was employed. The morphological peculiarities were examined by the scanning electron microscopy method (SEM) on a Tescan Vega Compact microscope with an EDS X-max Oxford Instruments. To confirm the change in band gap, the UV-Vis-NIR spectrum in the wavelength range of 190 – 1400 nm ($BaSO_4$ was used as the standard) of compound $Sr_2Mn_{0.4}Ti_{0.6}O_4$ was recorded using Shimadzu UV-2600 (Japan) spectrophotometer.

HQ working solution was prepared immediately before the experiment. 1.0 cm^3 of the initial hydroquinone solution with the concentration of $C(C_6H_4(OH)_2) = 1 \cdot 10^{-2}$ mol/dm^3, 1.5 cm^3 of 0.5 M Na_2SO_4 solution were placed in 25.0 cm^3 measuring flasks and brought to the mark with distilled water. The concentration of the working solution of hydroquinone is 4.0 – 10^{-4} mol/dm^3. Before the work, a calibration graph was fixed in the range of HQ concentrations $0.0 - 4.0 \cdot 10^{-4}$ mol/dm^3 by measuring the height of the anodic oxidation peak of HQ at 0 V. The solutions were transferred to a cell in which 50 mg of photocatalyst was previously added and exposed to radiation. UV irradiation of HQ solutions was carried out in quartz cells using a BUV-15 lamp ($\lambda_{\max} = 253$ nm). Oxidation under the blue lamp ($\lambda_{\max} = 440 - 460$ nm) was carried out in glass cells. The HQ content in the solution was controlled by voltammetry.

Voltammetric study of $Sr_2Mn_{0.4}Ti_{0.6}O_4$ samples was carried out with use of an electroactive carbon paste electrode (CPE). It consisted of a mixture of a substance to study, spectrally pure graphite with particles' size of ≤ 63 μm, and a binder (Vaseline oil), taken in a 1 : 9 : 3 weight ratio and had the working area of 0.07 cm^2. The reference electrode was a saturated silver-silver chloride electrode. The voltammograms were recorded in two polarization modes of CPE, in 0.5 M Na_2SO_4. Redox processes on the surface of the samples were investigated as follows. The reduction processes were fixed from $+0.6$ to -1.6 V, the oxidation processes were recorded from -1400 to $+600$ V. All measurements were realized by PU-1 polarograph at scan rate 30 mV/s.

3. Results and discussion

In the studied system of solid solutions $Sr_2Mn_xTi_{1-x}O_4$ ($T = 1200$ °C; $x = 0.05, 0.15, 0.25, 0.4$) according to XRD data, only the composition $Sr_2Mn_{0.4}Ti_{0.6}O_4$ is single phase (Fig. 1). The other samples contain SrO and TiO_2 as impurity phases.

In [14], during the preparation of Mn-dopping $SrTiO_3$, it was noted the presence of similar impurity phases, which was attributed by the authors to the formation of strontium carbonate. However, these impurities disappear at the highest possible Mn concentration, indicating that doping promotes the complete reaction. The absence of the MnO peak in the diffractograms means that it takes place the successful introduction of Mn into the lattice of $SrTiO_3$ [14]. In addition, the authors suggested the different valence state of manganese during the decomposition of the carboxylate complex, especially noticeable at small amounts of dopant [17, 18].

For further study, we have chosen a single-phase sample of $Sr_2Mn_{0.4}Ti_{0.6}O_4$. The diffractogram of the sample $Sr_2Mn_{0.4}Ti_{0.6}O_4$, indexed in space group I4/mmm (No. 139) is presented in Fig. 1b. Crystallochemical characteristics of Sr_2TiO_4 and $Sr_2Mn_{0.4}Ti_{0.6}O_4$ are summarized in Table 1.

The decrease of the cell parameters with decreasing the unit cell volume of doped strontium titanate $Sr_2Mn_{0.4}Ti_{0.6}O_4$ confirms the incorporation of the smaller Mn^{4+} ion (0.53 Å) into the octahedral positions occupied by the larger Ti^{4+} ion

TABLE 1. The crystallochemical parameters of Sr_2TiO_4 and $Sr_2Mn_{0.4}Ti_{0.6}O_4$ (space group I4/mmm, Sr (4e, 0; 0; z), Ti/Mn (2a, 0; 0; 0), O1 (4e, 0; 0.5; 0), O2 (4c, 0; 0; z))

	Sr_2TiO_4	$Sr_2Mn_{0.4}Ti_{0.6}O_4$
Cell parameters		
a, Å	3.883(4)	3.846(1)
c, Å	12.588(2)	12.562(5)
V, Å^3	189.894(3)	185.882(1)
Atom parameters		
Sr		
z, Å	0.354(7)	0.354(1)
O1		
Occupancy	0.979(5)	1.02(4)
O2		
z, Å	0.159(1)	0.160(1)
Occupancy	1.078(5)	1.01(4)
B_{iso}, Å^2		
Sr	0.317(2)	0.766(9)
Mn	—	0.616(2)
Ti	0.334(5)	0.616(2)
O1	0.546(1)	1.074(4)
O2	0.548(2)	1.433(4)
Selected bond lengths (Å)		
Ti/Mn – O1 ($\times 4$)	1.941(2)	1.923(1)
Ti/Mn – O2 ($\times 2$)	2.003(5)	2.018(8)
Sr – O1 ($\times 4$)	2.673(7)	2.653(7)
Sr – O2a ($\times 4$)	2.751(3)	2.726(5)
Sr – O2b ($\times 4$)	2.454(5)	2.434(3)
R-factors		
R_{wp}, %	16.4	8.14
R_{exp}, %	11.6	10.13
R_p, %	10.6	5.79
R_f	3.83	3.82
χ^2	1.99	0.72

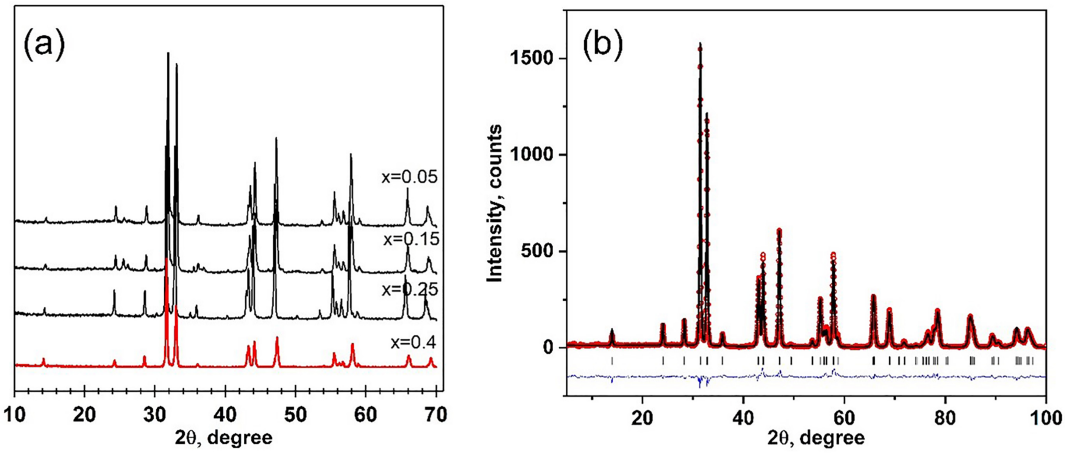

FIG. 1. (a) Diffractograms of $Sr_2Mn_xTi_{1-x}O_4$ ($x = 0.05, 0.15, 0.25, 0.4$); (b) Experimental ('○'), theoretical (black line) and difference (blue line) diffractograms of $Sr_2Mn_{0.4}Ti_{0.6}O_4$, ('|') are Miller indices

(0.605 Å) [19]. According to SEM data, the pyrolysis product of the reaction mass $Sr_2Mn_{0.4}Ti_{0.6}O_4$ consists of nanoscale particles (Fig. 2a).

After annealing in the indicated temperature range, agglomeration of crystallites up to 1 nm is observed. The results of EDAX study confirm the chemical composition of the compound. The uniform distribution of elements in the agglomerates is confirmed by EDS-mapping (Fig. 2b).

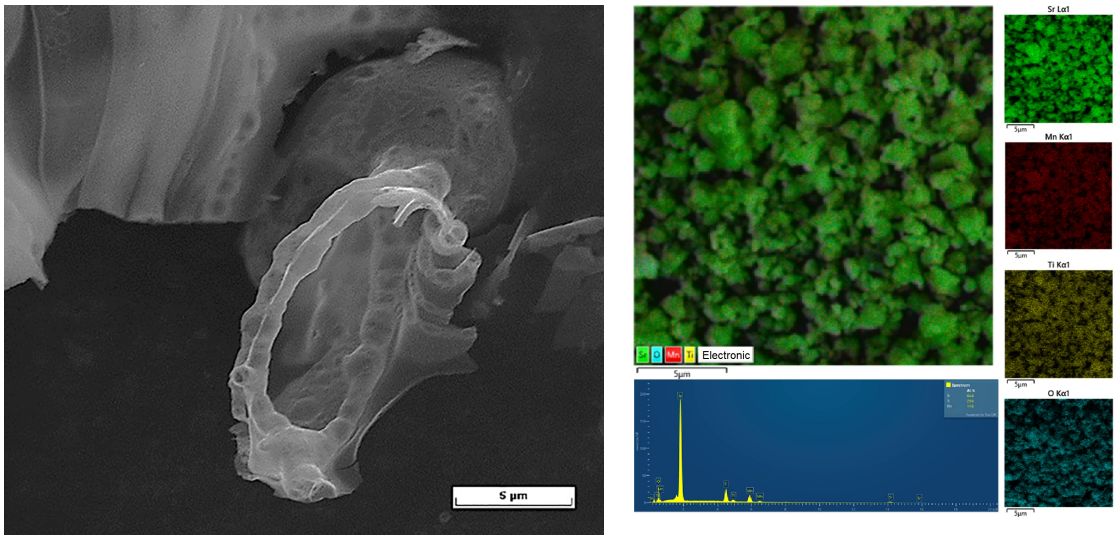

FIG. 2. SEM image of SHS-synthesis product (a) and EDS-mapping of $Sr_2Mn_{0.4}Ti_{0.6}O_4$, calcined at 1200 °C (b)

To establish the effect of the manganese dopant on the optical characteristics of Sr_2TiO_4, the optical absorption spectrum in the UV, visible and near-IR ranges was studied (Fig. 3a).

The absorption band at 459 nm is attributed to the $^4A_{2g} \rightarrow {}^4T_{2g}$ transition of the Mn^{4+} ion, and the shoulder near 300 nm is most likely associated with the $^4A_{2g} \rightarrow {}^4T_{1g}$ transition of the Mn^{4+} ion (Fig. 3a). The determination of the band gap is performed by the way of approximation of the absorption edge using the Tauc relation: $(\alpha h\nu)^2 = A(h\nu - E_g)$, where α is the absorption coefficient, $h\nu$ is the photon energy, E_g is the band gap, A is an independent constant. According to this equation, the optical band gap can be obtained by the extrapolation of the linear part of the $(\alpha h\nu)^2 = f(h\nu)$ to the intersection with the abscissa axis (Fig. 3b). The band gap for $Sr_2Mn_{0.4}Ti_{0.6}O_4$ is 1.8 eV.

To clarify the valence state of Mn in $Sr_2Mn_{0.4}Ti_{0.6}O_4$, EPR spectra and voltammetry (VA) data of the sample were investigated. To this date, there is no discussion about the nature and properties of Mn^{4+} centers in the STO crystal. It is generally accepted that tetravalent manganese ions isovalently replace the octahedrally coordinated position of titanium in the crystal. In this case, the ground state of Mn^{4+} ions is the orbital singlet $^4A_2$, i.e., the outer electron shell is characterized by a highly symmetric distribution d of electron density [17, 18]. In other words, Mn^{4+} ions should not

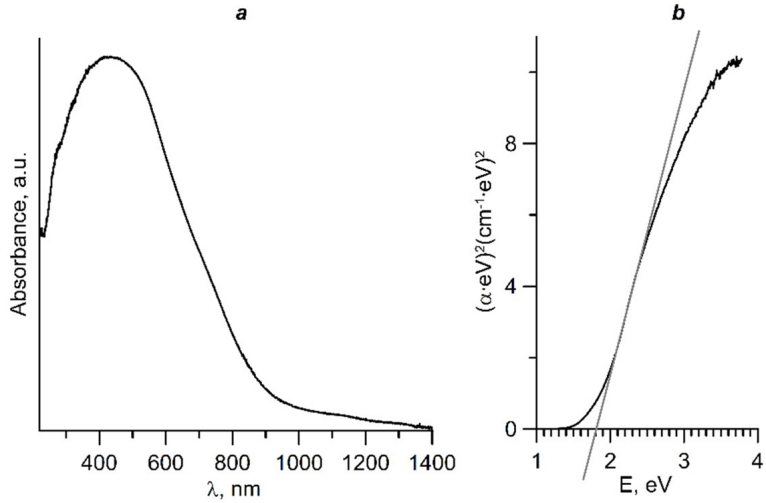

FIG. 3. (a) UV-Vis-NIR spectra of $Sr_2Mn_{0.4}Ti_{0.6}O_4$; (b) band gap E_g estimation using Tauc plot method

introduce a perturbation into the crystal lattice that would lead to a decrease in the symmetry of the center. Therefore, the structure of the EPR spectrum should reflect the symmetry of the crystal field.

Figure 4a shows the EPR spectrum of $Sr_2Mn_{0.4}Ti_{0.6}O_4$. The EPR spectrum is symmetric, well described by the Lorentz function. The parameters of the Lorentz curve are resonance field $H_{\text{res}} \approx 3379.9$ Oe, line width $\Delta_H \approx 173.2$ Oe, g-factor (having the value 1.99 which corresponds to the Mn^{4+} ion).

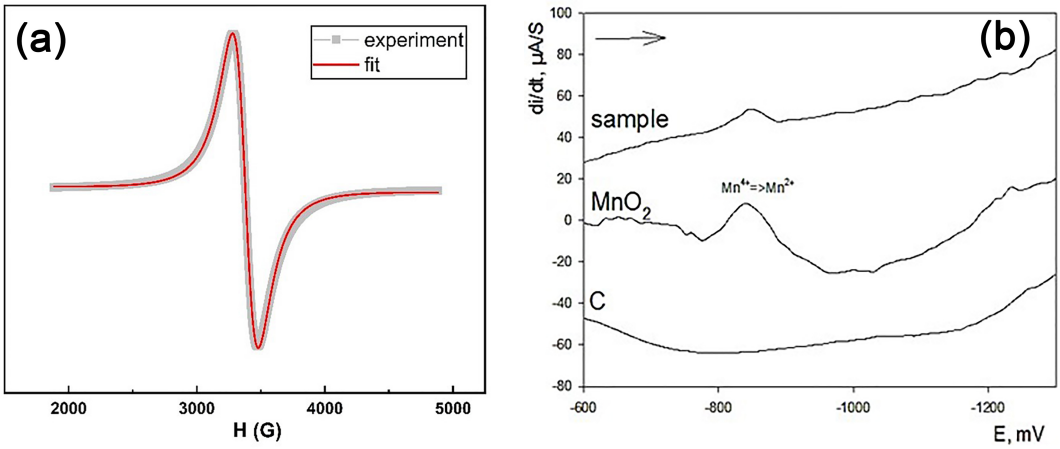

FIG. 4. (a) EPR spectra of $Sr_2Mn_{0.4}Ti_{0.6}O_4$; (b) Voltammetric recovery curves of $Sr_2Mn_{0.4}Ti_{0.6}O_4$, carbon and MnO_2; background electrolyte -0.5 M NH_4OH and 0.25 M Na_2SO_4

The value of g-factor is close to literature data for Mn^{4+} ions, both for highly concentrated and low concentrated compounds [20–23]. The absence of Mn^{4+} ion hyperfine structure in the EPR spectrum of $Sr_2Mn_{0.4}Ti_{0.6}O_4$ may be due to exchange interactions between manganese ions.

Voltammetry data confirm the presence of Mn^{4+} (Fig. 4b). The VA behavior of Mn(IV) oxide was preliminarily studied. At cathodic wave of MnO_2 at -850 mV, one can see the reduction peak, that corresponds to the Mn(IV) reduction to Mn(II). A similar signal is recorded on voltammetry of $Sr_2Mn_{0.4}Ti_{0.6}O_4$ (Fig. 4b). From the analysis of the obtained polarization curves, it can be concluded that manganese in the studied sample $Sr_2Mn_{0.4}Ti_{0.6}O_4$ is initially in the form of Mn^{4+}.

According to UV-Vis-NIR spectroscopy data, the narrowing of the band gap of $Sr_2Mn_{0.4}Ti_{0.6}O_4$ (1.8 eV) compared to Sr_2TiO_4 (3.16 eV) indicates a significant shift of the photosensitivity of the compound to the visible range of the spectrum.

The photocatalytic activity of the samples was evaluated by the decomposition rate of the reference organic compound 1.4-dihydroxybenzene (hydroquinone, HQ). The sample was found to exhibit high photocatalytic activity in both light ranges (Fig. 5).

The stability of the catalyst performance was tested in three consecutive oxidation cycles for 6 hours (Fig. 5b). The photoefficiency of $Sr_2Mn_{0.4}Ti_{0.6}O_4$ increases with increasing the number of cycles performed. Table 2 shows the values

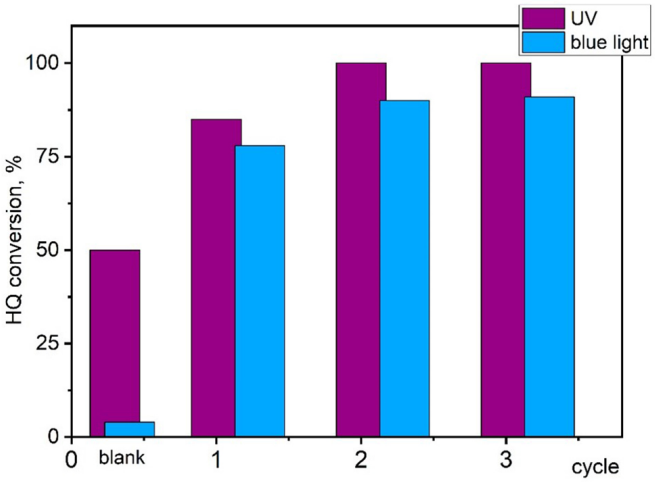

FIG. 5. Decrease in HQ concentration without catalyst (blank) and on $Sr_2Mn_{0.4}Ti_{0.6}O_4$ as a function of irradiation type and cycling for 6 h

of the rate constants of the oxidation reaction of HQ under UV and visible light. Kinetic equations for the 1st order reaction were used. The main kinetic parameters of the investigated sample were compared with the commercial catalyst Degussa P25. The obtained data show that the photoefficiency of the catalyst $Sr_2Mn_{0.4}Ti_{0.6}O_4$ exceeds Degussa P25 on average 4 times at UV stimulation (Table 2).

The increase in the rate of photooxidation and stabilization of photocatalytic properties of $Sr_2Mn_{0.4}Ti_{0.6}O_4$ with increasing time of catalyst operation in HQ working solutions can be related to activation of its working surface during the first oxidation cycle. Therefore, to increase the efficiency of the catalyst before use, it should be pre-soaked for 4 – 6 hours in a working solution of hydroquinone. The approximate mechanism of photooxidation of organic substances on strontium titanates was discussed in a number of works [14–19]. Upon light stimulation of ZnO particles, photoinduced electrons migrate to the conduction band (CB), while photoinduced holes remain in the valence band (VB). The doping impurity cations (Mn) actively participate in the separation of the formed exciton e^-/h^+ pair. In addition, manganese directly interacts with oxygen adsorbed on the surface of $Sr_2Ti(Mn)O_4$. Other probable electron/hole trapping sites are charged oxygen vacancies (VO^+, VO^{2+}) [24]. As a result, various reactive oxygen species (ROS) such as hydroxyl and superoxide radicals (•HO and $•O_2-$), extremely active oxidizing agents, are formed in the reaction zone. These ROS subsequently participate in the oxidation of HQ.

High photoactivity of $Sr_2Mn_{0.4}Ti_{0.6}O_4$ in HQ solutions indirectly indicates the formation of superoxide radical $•O_2-$ on its working surface in the first place. In practice, the radical trap addition method is used to determine the type of

TABLE 2. Value of rate constants of HQ photooxidation reaction (k_s) and HQ half-life (τ) in the presence of photocatalysts Degussa P25 and $Sr_2Mn_{0.4}Ti_{0.6}O_4$

Catalyst	$\lambda_{max} = 253$ nm				$\lambda_{max} = 440 – 460$ nm		
	$k_s \cdot 10^5$, s^{-1} ($n = 7$, $P = 0.95$)*	$S \cdot 10^5$ **	ε, % ***	τ, h	$k_s \cdot 10^5$, s^{-1}	$S \cdot 10^5$	τ, h
HQ blank.	1.34±0.12	0.11	8.9	14.4	0.15	0.03	132
Degussa P25	4.37±0.65	0.57	15.0	4.9	—	—	—
$Sr_2Mn_{0.4}Ti_{0.6}O_4$					$Sr_2Mn_{0.4}Ti_{0.6}O_4$		
1st cycle	10.70±7,22	5.20	6.7	1.8	7.18±2.34	1.32	2.7
2nd cycle	18.62±2.86	1.15	15.3	1.0	8.09±4.37	3.52	2.4
3rd cycle	18.90±2.90	5.21	6.8	1.0	7.72±2.67	2.16	2.5

*Sample number n at confidence coefficient P;

**Standard deviation;

***Relative error of the average value of k_s.

radicals. One of the most effective superoxide radical scavengers is the HQ derivative benzoquinone (BQ) [25]. According to our studies, the photoactivity of $Sr_2Ti_{1-x}M_xO_4$ (M = Mn, Cu) in the extended spectral range with respect to HQ oxidation exceeds essentially the known analogs [4–12]. Thus solid solutions $Ti_{1-x}Mn_xO_{2-x}$ ($0.003 \leq x \leq 0.016$) with spherical aggregate morphology degrade HQ by 100 % in 11 h of operation ($\tau = 5.5$) in the UV and in 12 h ($\tau = 6$) with 90 % yield in blue light [26]. The use of Sr_2TiO_4-based solid substitution solutions reduces the oxidation time of aromatic compounds: for comparison, $Sr_2Mn_{0.4}Ti_{0.6}O_4$ decomposes HQ by 100 % in blue light in 5 h ($\tau = 2.5$). This result makes $Sr_2Ti_{1-x}Mn_xO_4$ promising targets for photooxidative catalysis in the visible light range.

4. Conclusion

Mn-doped Sr_2TiO_4 samples were prepared by SHS method with different concentrations of Mn: 5, 15, 25 and 40 mol%. XRD results indicate that the sample with maximum manganese concentration of $Sr_2Mn_{0.4}Ti_{0.6}O_4$ is the single phase in this system. According to the results of voltammetry, EPR, UV-Vis-NIR spectroscopy, Mn in the compound appears in the oxidation degree (4+), and the forbidden band of $Sr_2Mn_{0.4}Ti_{0.6}O_4$ narrows to 1.8 eV.

A study of the catalytic properties of $Sr_2Mn_{0.4}Ti_{0.6}O_4$ in HQ solutions showed its photoefficiency in the UV and visible light ranges during 3 consecutive photooxidation cycles. Moreover, the photooxidation rate of HQ upon irradiation with blue light is as close as possible to that in the UV range. These results are unexpected for Sr_2TiO_4 and require further investigation.

References

[1] Liu B., Li L., Liu X.Q., et al. $Sr_{n+1}TinO_{3n+1}$ ($n = 1, 2$) microwave dielectric ceramics with medium dielectric constant and ultra-low dielectric loss. *J. of the American Ceramic Society*, 2017, **100** (2), P. 496–500.

[2] Lu L.W., Lv M.L., Wang D., et al. Efficient photocatalytic hydrogen production over solid solutions $Sr_{1-x}Bi_xTi_{1-x}Fe_xO_3$ ($0 \leq x \leq 0.5$). *Applied Catalysis B – Environmental*, 2017, **200**, P. 412–419.

[3] Lu L.W., Lv M.L., Liu G., et al., Photocatalytic hydrogen production over solid solutions between $BiFeO_3$ and $SrTiO_3$. *Applied Surface Science*, 2017, **391**, P. 535–541.

[4] Sorkh-Kaman-Zadeh A., Dashtbozorg A. Facile chemical synthesis of nanosize structure of Sr_2TiO_4 for degradation of toxic dyes from aqueous solution. *J. Molecular Liquids*, 2016, **223**, P. 921–926.

[5] Chupakhina T.I., Eremina R.M., Gyrdasova O.I., et al. Perovskite-like $La_xSr_{2-x}Ti_{1-x/2}Cu_{x/2}O_4$ ($x = 0.2, 0.3, 0.5$) oxides with the K_2NiF_4-type structure active in visible light range: new members of the photocatalyst family. *J. of the Korean Ceramic Society*, 2024, **61** (5).

[6] Skvortsova L.N., Chukhlomina L.N., Gormakova N.A., et al. Investigation of B-N-Fe and Si-N-Fe catalysts ability to remove phenol compounds from water in presence of ozone and UV irradiation. *Vestnik Tomskogo Gosudarstvennogo Universiteta*, 2013, **370**, P. 190–193.

[7] Sobczynski A., Duczmal L., Zmudzinski W., Phenol destruction by photocatalysis on TiO_2: an attempt to solve the reaction mechanism. *J. Molecular Catalysis A – Chemical*, 2004, **213** (2), P. 225–230.

[8] Chen X.B., Shen S.H., Guo L.J., et al. Semiconductor-based Photocatalytic Hydrogen Generation. *Chemical Reviews*, 2010, **110** (11), P. 6503–6570.

[9] Sun X.Q., Xie Y.H., Wu F.F., et al. Photocatalytic Hydrogen Production over Chromium Doped Layered Perovskite Sr_2TiO_4. *Inorganic Chemistry*, 2015, **54** (15), P. 7445–7453.

[10] Sun X.Q., Xu X.X. Efficient photocatalytic hydrogen production over La/Rh co-doped Ruddlesden-Popper compound Sr_2TiO_4. *Applied Catalysis B – Environmental*, 2017, **210**, P. 149–159.

[11] Sun X.Q., Mi Y.L., Jiao F., et al. Activating Layered Perovskite Compound Sr_2TiO_4 via La/N Codoping for Visible Light Photocatalytic Water Splitting. *ACS Catalysis*, 2018, **8** (4), P. 3209–3221.

[12] Yu J.X., Xu X.X. Fluorination over Cr doped layered perovskite Sr_2TiO_4 for efficient photocatalytic hydrogen production under visible light illumination. *J. of Energy Chemistry*, 2020, **51**, P. 30–38.

[13] Pany S., Nashim A., Parida K. Titanium-Based Mixed Metal Oxide Nanocomposites for Visible Light-Induced Photocatalysis. *Nanocomposites for Visible Light-Induced Photocatalysis*, 2017, P. 295–331.

[14] Iriani Y., Afriani R., Sandi D.K., et al. Co-precipitation Synthesis and Photocatalytic Activity of Mn doped $SrTiO_3$ for the Degradation of Methylene Blue Wastewater. *Evergreen Joint J. of Novel Carbon Resource Sciences & Green Asia Strategy*, 2022, **9** (4), P. 1039–1045.

[15] Patial S., Hasija V., Raizada P., et al. Tunable photocatalytic activity of $SrTiO_3$ for water splitting: Strategies and future scenario. *J. Environmental Chemical Engineering*, 2020, **8** (3), 103791.

[16] Chupakhina T.I., Deeva Y.A., Melnikova N.V., et al. Synthesis, structure and dielectric properties of new oxide compounds $Ln_{1-x}Sr_{1+x}Cu_{x/2}Ti_{1-x/2}O_4$ (Ln = La, Pr, Nd) belonging to the structural type of K_2NiF_4. *Mendeleev Communications*, 2019, **29** (3), P. 349–351.

[17] Thanh T.D., Phan T.L., Oanh L.M., et al. Influence of Mn doping on the crystal structure, and optical and magnetic properties of $SrTiO_3$ compounds. *IEEE Trans. Magn.*, 2014, **201450**, P. 1–4.

[18] Mansoor H., Harrigan W.L., Lehuta K.A., et al. Reversible Control of the Mn Oxidation State in $SrTiO_3$ Bulk Powders. *Front. Chem.*, 2019, **7** (353), P. 1–8.

[19] Shannon R.D., Prewitt C.T. Effective ionic radii in oxides and fluorides. *Acta Crystallogr. B*, 1969, **25** (5), P. 925–946.

[20] Huber D.L. Linear temperature dependence of electron spin resonance linewidths in $La_{0.7}Ca_{0.3}MnO_3$ and $YBaMn_2O_6$. 2013, arXiv:1309.6353.

[21] Schaile S., et al. Korringa-like relaxation in the high-temperature phase of A-site ordered $YBaMn_2O_6$. *Physical Review B*, 2012, **85** (20), 205121.

[22] Stoyanova R., Zhecheva E., Vassilev S. Mn^{4+} environment in layered Li $[Mg_{0.5-x}Ni_xMn_{0.5}]O_2$ oxides monitored by EPR spectroscopy. *J. Solid State Chemistry*, 2006, **179** (2), P. 378–388.

[23] Li K., et al. Achieving efficient red-emitting $Sr_2Ca_{1-\delta}Ln_\delta WO_6$: Mn^{4+} (Ln= La, Gd, Y, Lu, $\delta = 0.10$) phosphors with extraordinary luminescence thermal stability for potential UV-LEDs application via facile ion substitution in luminescence-ignorable Sr_2CaWO_6: Mn^{4+}. *ACS Materials Letters*, 2020, **2** (7), P. 771–778.

[24] Zheng W.C., Wu X.X. Studies of EPR g factors of the isoelectronic $3d^3$ series Cr^{3+}, Mn^{4+} and Fe^{5+} in $SrTiO_3$ crystals. *J. of Physics and Chemistry of Solids*, 2005, **66** (10), P. 1701–1704.

[25] Tan H., Zhao Z., Zhu W.B., et al. Oxygen vacancy enhanced photocatalytic activity of pervoskite $SrTiO_3$. *ACS Appl. Mater. Interfaces*, 2014, **6**, P. 19184–19190.

[26] Wang Zh., Murugananthan M., Zhang Ya. Graphitic carbon nitride based photocatalysis for redox conversion of arsenic(III) and chromium(VI) in acid aqueous solution. *Applied Catalysis B – Environmental*, 2019, **248**, P. 349–356.

[27] Baklanova I.V., Krasil'nikov V.N., Gyrdasova O.I., & Buldakova L.Y. Synthesis and optical and photocatalytic properties of manganese-doped titanium oxide with a three-dimensional architecture of particles. *Mendeleev Communications*, 2016, **26**, P. 335–337.

Submitted 17 June 2024; revised 13 August 2024; accepted 14 August 2024

Information about the authors:

Tatyana I. Chupakhina – Institute of Solid State Chemistry UB RAS, Pervomayskaya, 91, Ekaterinburg, 620990, Russia; ORCID 0000-0002-1317-3803; chupakhina@yandex.ru

Olga I. Gyrdasova – Institute of Solid State Chemistry UB RAS, Pervomayskaya, 91, Ekaterinburg, 620990, Russia; ORCID 0000-0002-0680-6094; gyrdasova@ihim.uran.ru

Anastasya M. Uporova – Institute of Solid State Chemistry UB RAS, Pervomayskaya, 91, Ekaterinburg, 620990, Russia; ORCID 0009-0006-1219-8909; nastyauporova99@gmail.com

Larisa Y. Buldakova – Institute of Solid State Chemistry UB RAS, Pervomayskaya, 91, Ekaterinburg, 620990, Russia; ORCID 0000-0003-3642-7121; buldakova@ihim.uran.ru

Mikhail Y. Yanchenko – Institute of Solid State Chemistry UB RAS, Pervomayskaya, 91, Ekaterinburg, 620990, Russia; ORCID 0000-0001-8306-906X; yanchenko@ihim.uran.ru

Dzhavid V. Mamedov – Zavoisky Physical-Technical Institute, FRC Kazan Scientific Center of RAS, Kazan, 420029, Russia; javi-m@yandex.ru

Yulia A. Deeva – Institute of Solid State Chemistry UB RAS, Pervomayskaya, 91, Ekaterinburg, 620990, Russia; ORCID 0000-0003-1207-7331; juliahik@mail.ru

Inna V. Baklanova – Institute of Solid State Chemistry UB RAS, Pervomayskaya, 91, Ekaterinburg, 620990, Russia; ORCID 0000-0002-5643-7004; inna.b@bk.ru

Conflict of interest: the authors declare no conflict of interest.